



# Hydraulics of Linear-Move Sprinkler Irrigation Systems, III: Model Evaluation

Zerihun D<sup>1\*</sup>, Sanchez CA<sup>2</sup>, Thorp KR<sup>3</sup> and Hagler MJ<sup>4</sup>

<sup>1</sup>Maricopa Agricultural Center, University of Arizona, 37860, W. Smith-Enke Rd, Maricopa, AZ 85138-3010, USA

<sup>2</sup>Department of Soil, Water, and Environmental Science, Maricopa Agricultural Center, University of Arizona, 37860, W. Smith-Enke Rd, Maricopa, AZ 85138-3010, USA

<sup>3</sup>USDA-ARS Arid Land Agricultural Research Center, 21881 North Cardon Lane, Maricopa, AZ 85138, USA

<sup>4</sup>USDA-ARS Arid Land Agricultural Research Center, 21881 North Cardon Lane, Maricopa, AZ 85138, USA

## Abstract

This is the third manuscript of a three-part paper that presents the development and evaluation of a hydraulic simulation model for linear-move laterals equipped with pressure reducing valve (*prvs*). System description, model assumptions, and specification of the lateral hydraulic simulation problem are discussed in part-one of the paper. Formulation and numerical solution of the lateral hydraulic simulation problem are described in manuscript-two. Results of model evaluation and simulation examples, showing model applications, are presented here. Measured hydraulic data-sets, consisting of lateral pressure head profiles and inlet discharges, were used in model evaluation. The data was obtained through field tests conducted on a linear-move sprinkler irrigation system fitted with *prvs*. Comparisons of model-predicted and field-measured lateral pressure head profiles and lateral inlet discharges suggest that model performance is satisfactory. Furthermore, potential applications of the model in analyzing *prv*-set pressure effects on lateral hydraulics and, possibly, in the selection of a suitable *prv*-set pressure for a lateral with a given parameter combination is shown using simulation examples.

**Keywords:** Linear-move; Model evaluation; Span geometry; Lateral-wide operating scenarios of *prvs*; Lateral elevation profile

## Notations

$h_{min}$ : Minimum required *prv*-inlet pressure for the *prv* to function reliably in the active mode [L];

$h_{max}$ : Maximum recommended *prv*-inlet pressure for the *prv* to operate reliably in the active mode [L];

$h_{prv}$ : *prv*-set pressure [L];

$h_u$ : *prv*-inlet pressure [L];

$\delta h_{prv}$ : Minimum recommended pressure head margin between  $h_u$  and  $h_{prv}$  for the *prv* to function reliably [L];

*prv*: Pressure reducing valve [-];

$Q_s$ : Sprinkler discharge [ $L^3/T$ ].

## Introduction

Linear-move sprinkler irrigation systems are used to irrigate a wide variety of crops [1] at high levels of application efficiency [2]. Because of their amenability to automation linear-move systems are particularly suitable for variable rate application of water and agricultural chemicals and have minimal labor requirements. Furthermore, these systems are often outfitted with appurtenances that minimize energy consumption and allow better control of water application. Owing to these advantages, the irrigated acreage that is under linear-move systems is expanding. Thus, the availability of models that can be used in the hydraulic analysis, design, and management of these systems has become increasingly important.

Hydraulic modeling of irrigation laterals is typically based on analytical formulations. Equations, derived based on simplifying assumptions, have been used in the evaluation of friction head losses and pressure head profiles of solid-set and set-move sprinkler irrigation laterals [3-5]. Analytical formulations and simplified numerical approaches were also used in hydraulic analysis of center-pivot and linear-move irrigation systems [6-13].

Availability of improved computational resources have allowed the development of more accurate and versatile numerical simulation

models of solid-set and set-move irrigation laterals [14-16]. However, the subject of the current study is the development and evaluation a hydraulic simulation model for linear-move irrigation system laterals equipped with pressure reducing valves, *prvs*. This manuscript is the third of a three-part paper. System configuration and components, model assumptions, and definition of the hydraulic simulation problem are discussed in part-one of the paper. The second part of the paper describes the formulation of the linear-move lateral hydraulic simulation problem and numerical solutions. Results of model evaluation and potential applications of the model are presented here.

Model evaluation was conducted based on comparison of model outputs with measured hydraulic data, consisting of lateral pressure head profiles and inlet discharges. The hydraulic data was obtained through field tests performed on a linear-move sprinkler irrigation system equipped with *prvs*. Results of model evaluation suggest that model performance is satisfactory. Furthermore, potential applications of the model in analyzing *prv*-set pressure effects on lateral hydraulics and, possibly, in the selection of an acceptable *prv*-set pressure for a lateral with a given combination of hydraulic, geometric, and elevation profile characteristics are shown here using simulation examples.

## Model Evaluation

The hydraulic model developed here produces a range of outputs, given the hydraulic, geometric, and elevation data of a linear-move sprinkler irrigation system as input. The specific input data items include lateral pipe segment lengths and lateral elevation profiles (both defined along the centerline of a lateral), drop-tube lengths, pipe relative roughness, *prv* parameters, sprinkler parameters, local

**\*Corresponding author:** Zerihun D, Associate Research Scientist, Maricopa Agricultural Center, University of Arizona, 37860, W. Smith-Enke Rd, Maricopa, AZ 85138-3010, USA, Tel: +15203746221, +15209828797; E-mail: [dawit@ag.arizona.edu](mailto:dawit@ag.arizona.edu)

**Received** May 15, 2019; **Accepted** June 25, 2019; **Published** July 02, 2019

**Citation:** Zerihun D, Sanchez CA, Thorp KR, Hagler MJ (2019) Hydraulics of Linear-Move Sprinkler Irrigation Systems, III: Model Evaluation. Irrigat Drainage Sys Eng 8: 237.

**Copyright:** © 2019 Zerihun D, et al. This is an open-access article distributed under the terms of the Creative Commons Attribution License, which permits unrestricted use, distribution, and reproduction in any medium, provided the original author and source are credited.

head loss coefficients, and total head at the lateral inlet (Table 1). The main outputs of the numerical model are the link discharge vector (lateral pipe segment and sprinkler discharges),  $Q$ , and total heads just upstream of each junction node,  $H$ . Additional model outputs include velocity heads and friction head losses in each of the lateral pipe segments, local head losses, piezometric head profile along the lateral, lateral pressure head profile, inlet and outlet pressures of each *prv*, *prv* operating mode (active and/or passive), and head differential across each sprinkler.

Model evaluation was conducted based on comparison of model outputs with measured hydraulic data. The data was obtained through field tests performed on a linear-move sprinkler irrigation system comprised of a series of vertically arched spans, each with multiple outlets ports placed at variable spacing. The system obtained its water supply from a concrete-lined canal and was operated under steady flow conditions. Spray nozzles, alternatively referenced here simply as sprinklers, were used to apply water along the lateral. To maintain a set-pressure upstream of the spray nozzles, each nozzle was coupled to a *prv* at its inlet end. Drop-tubes were used to convey water from the overhead outlet ports down to each *prv*-sprinkler assembly. Three hydraulic data-sets, consisting of lateral pressure head profiles and inlet discharges, were obtained through the field measurements. One of the data sets was used in parameter estimation and the remaining two were used in model verification, i.e., comparison of measured and simulated lateral pressure head profiles and inlet discharges. Descriptions of the linear-move sprinkler irrigation system used in the study, field measurements, and results of model evaluation are presented below.

### Description of the sprinkler system used in model evaluation

Irrigation field evaluations were conducted in the spring of 2018 on a linear-move sprinkler irrigation system installed on the research

farm of the Maricopa Agricultural Center of the University of Arizona, Maricopa, AZ. The linear-move system was managed by the USDA-ARS Arid-Land Agricultural Research Center, Maricopa, AZ. The irrigated field, which covers an area of approximately 6 ha, was laser leveled in the weeks before the field evaluations. The lateral was 365.3 m long (i.e., referring to the horizontal distance between the inlet- and distal-ends of the lateral). However, the effective length of the lateral considered for hydraulic modeling purpose was 361.7 m. It covered the horizontal distance between a point on the lateral just upstream of the first sprinkler, which is treated here as the lateral inlet, and the distal-end outlet of the lateral.

The lateral had seven spans and, as noted earlier, it obtained its water supply from a concrete-lined canal (Figure 1). Span lengths were variable along the lateral. Note that in subsequent discussions, the spans that make up the lateral are numbered sequentially starting from the upstream-end span, which is referred to here as span 1, and increasing in the downstream direction along the lateral. The length of span 1 was 54.5 m. However, the effective length considered here for modeling was 50.8 m (Figure 1). Spans 2 to 6 were each 56.8 m long. The effective length of span 7 was 27 m, which was the distance of the distal-end outlet on the lateral from the span inlet. Each of spans 1 to 6 were supported at both ends with wheeled towers. Span 7, on the other hand, was a cantilever type beam, commonly referred to as an overhang, and was supported only at its inlet end. The machine was powered by a diesel engine placed on the support-tower at the inlet-end of span 1. This tower travelled on an elevated track along the berm of an embankment of the field supply canal, but the tower attached to the distal-end of the span had its wheels on the field surface (Figure 1). Hence, the upstream-end span was inclined at an appreciable negative slope between its inlet- and distal-ends. By comparison, spans 2 to 7 were all operated on a level field. Based on machine specification data [17] and field observations, it was deemed that spans 2 to 6 had

| Lateral parameters                                      |                    | Units | Data-set <sup>(a)</sup> |   |   |
|---|--------------------|-------|-------------------------|---|---|
|   |                    |       | 1                       | 2 | 3 |
| Number of spans   |                    | -     | 7                       |   |   |
| Effective span length <sup>(b)</sup>                    |                    | m     | 27, 50.8, and 56.8      |   |   |
| Lateral length  | Horizontal         | m     | 361.7                   |   |   |
|   | along center-line  | m     | 362.0                   |   |   |
| Support tower height                                    |                    | m     | 3.7                     |   |   |
| Elev. differential between span joint and field surface |                    | m     | 3.62                    |   |   |
| Maximum in-span elevation differentials <sup>(c)</sup>  |                    | m     | 0.65(0.74)/1.15/1.50    |   |   |
| Lateral diameter <sup>(d)</sup>                         |                    | mm    | 162.3/136.4/101.6       |   |   |
| Absolute roughness                                      | Lateral pipe       | mm    | 0.0015                  |   |   |
|   | Drop-tube          | mm    | 0.0015                  |   |   |
| Drop-tube length range                                  |                    | m     | 2.6-4.4                 |   |   |
| Drop-tube diameter                                      |                    | mm    | 19.05                   |   |   |
| Field surface slope                                     |                    | %     | 0.0                     |   |   |
| Local head loss parameters                              | branching, outlet  | -     | 0.03                    |   |   |
|   | line-flow, outlet  | -     | 0.008                   |   |   |
|   | bending, connector | -     | 0.02                    |   |   |
|   | span joints        | -     | 0.04                    |   |   |
| Reduction <sup>(e)</sup>                                |                    | -     | 0.104/0.195             |   |   |
| Constant total head at the inlet <sup>(f)</sup>         |                    | m     | 19.2, 23.4, and 27.7    |   |   |
| Elev. at the inlet                                      |                    | m     | 4.84                    |   |   |

**Table 1:** Lateral hydraulic, geometric and elevation data used in model evaluation.

<sup>(a)</sup>Data-sets 1, 2, and 3 pertain to an actual linear-move system with six full spans and a cantilever type beam at its downstream-end. Thus, all the lateral parameters are the same for these data-sets except the total head at the inlet. <sup>(b)</sup>Effective span lengths, i.e., lengths considered for modeling purpose, are 50.8 m for the inlet-end span, 56.8 m for spans 2 to 6, and 27 m for the distal-end span. <sup>(c)</sup>The maximum in-span elevation differentials of the lateral are: 1.5 m for the upstream-end span and 1.15 m for spans 2 to 6. For span 7, the maximum elevation differentials are 0.65 m during irrigation and 0.74 m when the lateral is idle. <sup>(d)</sup>The linear-move system has a diameter of 162.3 mm over spans 1 to 6, span 7 has a diameter of 136.4 mm over the upper 13.8 m segment of the span and has a diameter of 101.6 mm over the lower 13.2 m long section of the span. <sup>(e)</sup>The local head loss coefficients for lateral diameter reductions are obtained from Granger based on pipe diameter ratios. <sup>(f)</sup>The inlet heads for data-sets 1, 2, and 3 are 19.2, 23.4, and 27.7 m, respectively.

the same geometry. In other words, they had the same length and same maximum in-span elevation differential. Furthermore, a curve tracing the centerline of each of these spans was considered here to be symmetric about a vertical line through the span's mid-point. Evidently, the elevation profile, of each of spans 1 to 6, had a concave form (Figure 1). Thus, for these spans the point of maximum in-span elevation occurred somewhere in between the inlet and distal-end of the spans (Figure 1). In contrast to spans 1 to 6, the elevation profile of span 7 was a convex curve and the point of maximum in-span elevation occurred at the distal-end of the span, and the minimum was somewhere between the inlet and distal-ends of the span [17].

Except for span 7, pipe diameter was constant along the lateral. A diameter of 162.3 mm (6.39") was used over spans 1 to 6 (Table 1). Lateral diameter was then reduced to 136.4 mm (5.37") over the upper 13.8 m long reach of span 7. It was reduced further to 101.6 mm (4.0") over the distal 13.2 m long section of the span. The lateral had a total of 349 sprinklers, with 49 sprinklers in span 1; 55 sprinklers each on spans 2, 4, 5, and 6; 53 sprinklers on span 3; and 27 sprinklers on span 7. The sprinkler model used in this lateral was Super spray UP3 produced by Senninger [18]. The nozzle size was 4.76 mm (3/16"). The coefficient and exponent of the hydraulic characteristic function of the sprinkler, obtained based on head-discharge data provided in the manufacturer's catalogue, is summarized in Table 2. A pressure reducing valve, *prv*, was attached to the inlet-end of each sprinkler. The *prv* model used in this lateral was PSR2 [19]. The *prv*-set pressure,  $h_{prv}$ ; the maximum allowable inlet pressure for the *prv* to operate reliably in the active mode,  $h_{max}$ ; and the minimum required pressure head margin between

the set pressure and the inlet pressure for the *prv* to operate reliably in the active mode,  $\delta h_{prv}$ , are summarized in Table 2. Drop-tube lengths vary between 2.6 and 4.4 m and they were set such that each *prv*-sprinkler assembly was suspended from a lateral outlet at a uniform above ground clearance of about 0.76 m (2.5 ft), when the lateral was operated in a level field [18]. The drop-tubes had a constant diameter of 19.05 mm (3/4").

### Determination of lateral elevation profile

The elevation profile of span 1 was different from spans 2 to 6, mainly because of the differences in slopes. The profile of span 7 was also different from the spans upstream, because of the differences in the general concavity structure of the elevation profiles of span 7 and the other spans. As noted earlier, spans 2 to 6 had the same geometry and were operated on a level field, thus they had the same elevation profile. This implies that the elevation profile measured along any one of these spans should be applicable to the rest of the spans, after accounting for the differences in the horizontal distances of outlet-ports and span joints from the lateral inlet. Thus, determination of the elevation profile of the centerline of the entire lateral was made based on measurements over spans 1, 2, and 7 only. Accordingly, a profile survey was conducted over spans 1, 2, and 7 using the elevation of the field surface (which as noted earlier was considered horizontal) as datum. The measured elevation profile data for spans 1 and 2 were fitted to the equation of an ellipse and a cubic polynomial was fitted to the data for span 7, each with a coefficient of determination ( $r^2$ ) of 0.99. Note that the elevation profile of span 2 was used to define those of spans 3 to 6 as well. The

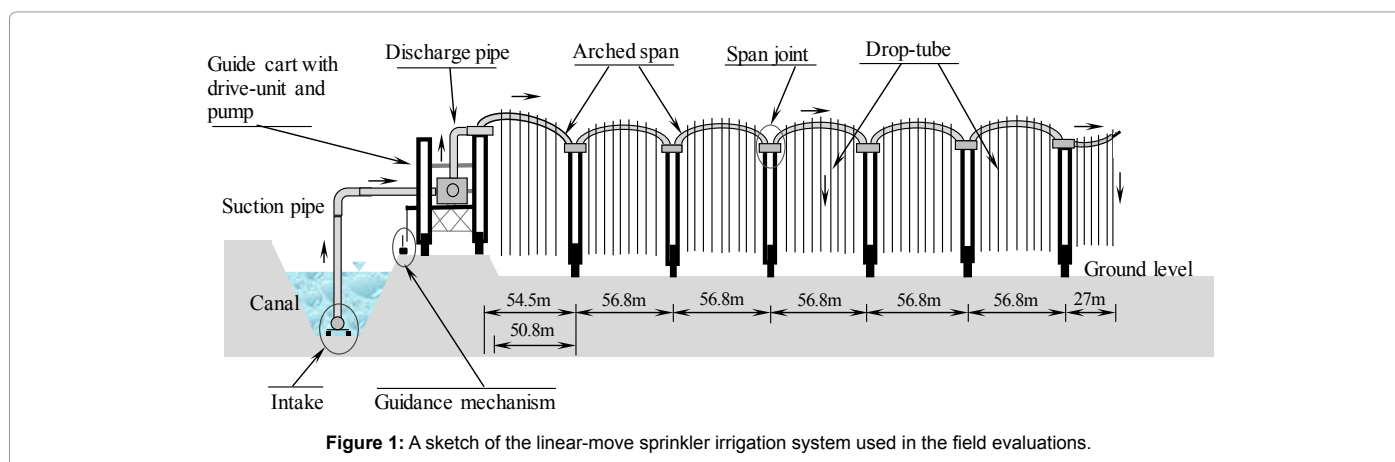


Figure 1: A sketch of the linear-move sprinkler irrigation system used in the field evaluations.

| Lateral parameters                                 |   | Units            | Data-set           |        |   |  |
|--|---|------------------|--------------------|--------|---|--|
|  |   |                  | 1                  | 2      | 3 |  |
| Number of <i>prvs</i> , sprinklers, and drop-tubes |   | -                | 349                |        |   |  |
| Sprinkler spacing, horizontal                      |   | m                | 0.59-1.65          |        |   |  |
| Sprinkler data                                     | Sprinkler model                                 | -                | Super spray UP3    |        |   |  |
|  | Nozzle size                                     | mm (in)          | 4.763 (3/16)       |        |   |  |
|  | Parameters of sprinkler head-discharge function | $\rho$           | L/s/m <sup>2</sup> | 0.0771 |   |  |
| $\lambda$  |   | -                | 0.4998             |        |   |  |
| <i>prv</i> data                                    | <i>prv</i> model                                | -                | PSR2               |        |   |  |
|  | <i>prv</i> parameters                           | $h_{prv}$        | m                  | 4.2    |   |  |
|  |   | $\delta h_{prv}$ | m                  | 3.5    |   |  |
| $h_{max}$  |   | m                | 90                 |        |   |  |

Table 2: Sprinkler and *prv* data of the linear-move system used in model evaluation.

Note:  $\rho$  and  $\lambda$  are coefficient and exponent, respectively, of the sprinkler head-discharge function and are derived through regression from the data provided in manufacturer's catalogue.  $h_{prv}$  is *prv*-set pressure head;  $\delta h_{prv}$  is the minimum required pressure head margin, between the *prv*-inlet pressure and  $h_{prv}$  in order for the *prv* to operate reliably in the active mode; and  $h_{max}$  is the maximum allowable pressure at the *prv* inlet for the *prv* to operate in the active mode.

lateral elevation profile defined in terms of the regression equations was used as model input.

The measured elevation profile showed that span 1 was inclined at an average slope of -1.7% between its inlet- and distal-ends. As a result, the point of maximum in-span elevation was upstream of the span mid-point and was located 15.7 m from the lateral inlet. The overall elevation increment from the lateral inlet (i.e., the location of the upstream end pressure gauge) to the highest point in the span was 0.3 m. However, the decrement in elevation over the lower 35.1 m long reach of span 1 was 1.5 m, which is five times the increment in elevation that occurred over the upstream section of the span. By contrast, the elevation profile of each of spans 2 to 6 can be considered symmetrical about a vertical line through the span mid-point. Thus, for each of these spans the increment in elevation over the upper-half was the same as the elevation decrement over the lower-half and was equal to 1.15 m. The elevation of the lateral centerline at the span joints (i.e., at points above the support towers) was 3.62 m. Note that elevation of lateral centerline was measured with respect to the field surface, which was slightly higher than the wheel tracks of the support towers due to compaction from previous passes of the machine.

Elevation profile measurements were made during an off-time, when the system was idling and parked at a fixed position. The elevation profiles of spans 1 to 6 were the same during irrigation as well as when the system was idling, because each of these spans were supported at both ends. By comparison, the elevation profile of span 7 differed slightly depending on whether the machine was idling or irrigating. The maximum elevation of span 7, measured when the system was idling, was 4.16 m and it occurred at the distal-end outlet of the span. The corresponding maximum in-span elevation differential was 0.74 m. However, during an irrigation event the elevation profile of this span, which was supported only at its inlet end, underwent a vertical deflection under the weight of the irrigation water. As a result, the maximum elevation of the span decreased to about 4.01 m and the corresponding maximum in-span elevation differential was 0.65 m. Furthermore, a close look at the elevation profile (geometry) of span 7 showed that it was not symmetrical about a vertical line through its mid-point. Span elevation decreased by 0.26 m over the upper 13.8 m long reach of the span and then increased by 0.65 m over the lower 13.2 m section of the span. Note that the rise in elevation over the lower section of the span was greater than the drop in elevation that occurred over the upper reach of the span by more than 2.5 times. Differences in the general concavity structure of the spans elevation profiles and the presence or lack of symmetry, in the span elevation profiles, about the mid-point of the spans have appreciable effects on the spatial trends of the lateral pressure head profiles. These effects are highlighted below in the context of model evaluation.

### **Irrigation field evaluations and determination of model parameters**

In the spring of 2018, three irrigation field evaluations were conducted on the linear-move system described above (data-sets 1, 2, and 3, Tables 1 and 2). The goal of the irrigation field evaluations was to collect lateral pressure head profile and inlet discharge data for model verification purposes. Accordingly, a total of thirty-two pressure gauges, five on each of spans 1 to 6 and two on span 7 were installed prior to the irrigation evaluations. Ten of the pressure gauges had data loggers and hence recorded pressure automatically at a preset time interval. Twenty-two of the pressure gauges were analog gauges. The gauges with data loggers were all installed in spans 2 and 3 and the analog gauges were installed on spans 1, 4, 5, 6 and 7. In order

to capture the effects of the in-span elevation differential on the span-scale pressure head variations, the five gauges installed in each of spans 1 to 6 were arranged as follows: one of the gauges was installed close to the span inlet, another one close to the distal-end of the span, and a third one was placed near the mid-point of the span. The remaining two gauges were installed at distances of about one-quarter and three-quarters of the span length from the span inlet. In span 7, the first gauge was placed close to the inlet-end of the span and the second gauge was placed near the span's mid-point, where elevation was minimum.

All system parameters, except for the total head at the lateral inlet, were kept constant during each of the evaluations. Prior to the start of each irrigation evaluation event, pressure at the discharge-end of the pump was adjusted to pre-determined levels by varying the opening of the valve. The pre-determined pressure heads at the pump were 16.2 m (23 PSI), 21.1 m (30 PSI), and 26 m (37 PSI) for data-sets 1, 2, and 3, respectively (Table 1). The corresponding total heads at the lateral inlet were 19.2, 23.4, and 27.7 m for data-sets 1, 2, and 3, respectively. Note that these refer to the total heads at the location of the upstream-end pressure gauge and were determined as a function of the measured lateral pressure heads, lateral inlet discharges, and lateral elevation. Once the pressure at the pump was adjusted to a pre-determined level, the system was operated for a minimum of 5 min before a field evaluation event began, to ensure that the flow reached a steady-state corresponding to the newly set inlet head.

Each field evaluation event lasted 20 min. At each station with an analog gauge, pressure readings were taken manually every 5 min. This resulted in a total of six data points per station per evaluation. The pressure gauges with data loggers, on the other hand, were preprogrammed to record pressure every minute, resulting in a total of twenty-one data points per station. For each irrigation evaluation event, the station averages were treated as the local steady state pressure head values. Furthermore, during a field evaluation event discharge at the lateral inlet was measured every 5 min with a digital flow meter built into the upstream end support-tower. The average lateral inlet discharge for an event was considered as the corresponding steady inflow rate into the lateral.

The field measured lateral pressure profiles and inlet discharges were used in model evaluation. Data-set 1 was used in parameter estimation and data-sets 2 and 3 were used in model verification. Lateral parameters estimated based on data-set 1 were lateral pipe absolute roughness and local head loss coefficients. To the best of authors' knowledge there is no modeling capability that solves the inverse problem of linear-move lateral hydraulics that can be readily used here to estimate the model parameters. Thus, a simple trial and error approach was used to obtain a parameter set that resulted in a reasonable match between the simulated and measured lateral pressure head profiles. Given a set of parameter estimates, visual comparison of the simulated and measured pressure head profiles was used to qualitatively assess the goodness of fit between the profiles. The parameter estimates obtained as such are summarized in Table 1. A simple error metric termed as percent absolute residuals or simply as absolute residuals was used to obtain a quantitative measure of the differences between model predictions and field measurements for the parameter set given in Table 1. Note that the absolute residuals of lateral pressure head profiles or inlet discharges were defined, respectively, as the difference between models predicted and measured pressure profiles or inlet discharges, expressed a percentage of those obtained through measurement.

As can be noted from Table 3, the absolute residuals between the simulated and measured lateral pressure head profiles of data-set 1 vary

between a minimum of 0.1% and a maximum of 10.9% and the average is 5.1%. Furthermore, the absolute residuals between the simulated and measured lateral inlet discharges of data-set 1 is 8.8% (Table 4). Results of model verification obtained, based on these parameter sets, are presented next.

### Results of model verification

**Linear-move lateral pressure head profile, local in-span patterns and inter-span trends:** Figures 2a and 2b depict a comparison of the measured and simulated lateral pressure head profiles. The simulated and measured pressure head profiles are shown as dashed-lines and circles, respectively, and the elevation profile of the lateral is depicted as solid-line. In contrast to the rather smooth pressure head profiles of solid-set and set-move sprinkler irrigation laterals, both the simulated and measured pressure head profiles of the linear-move lateral show a unique wavy pattern. As a result, the pressure head profiles of the linear-move lateral exhibit two distinct forms of spatial variability attributes, consisting of local span-scale variability patterns and broader inter-span/lateral-wide trends (shown in Figures 2a and 2b as dash-dot lines). The implication is that a complete characterization of the pressure head profiles of the lateral requires that both spatial variability attributes be assessed. As can be noted from Figures 2a and 2b, the in-span lateral pressure variability patterns have a convex form, over each of spans 1 to 6, and a concave form in span 7. It can, thus, be observed that the local in-span pressure variability patterns noted here are closely related to the elevation profile of the spans. On the other hand, the inter-span trends depict the broader spatial behavior of the lateral pressure head profiles, considered over multiple spans, and are related not only to span geometry but also to other parameters, including the slope of the field the lateral is installed in.

**Comparison of measured and simulated lateral pressure head profiles:** Visual observations of Figures 2a and 2b suggest that the simulated pressure head profiles of data-sets 2 and 3, for the most part, closely track the respective measured profiles. To provide a quantitative measure of the model prediction errors, the percent absolute residuals between the simulated and measured pressure head profiles are summarized in Table 3. Accordingly, the absolute residuals between the simulated and measured lateral pressure head profiles vary between 0.2 and 14.3% for data-set 2 and between 0.1 and 16% for data-set 3. The average absolute residuals of the lateral pressure head profiles are 3.7% for data-set 2 and 3% for data-set 3. The average absolute residuals obtained for both data-sets suggest a reasonably good agreement

| Absolute residuals | Units | Data-set |      |     |
|--------------------|-------|----------|------|-----|
|                    |       | 1        | 2    | 3   |
| Minimum            | (%)   | 0.1      | 0.2  | 0.1 |
| Average            | (%)   | 5.1      | 3.7  | 3   |
| Maximum            | (%)   | 10.9     | 14.3 | 16  |

**Table 3:** Residuals between measured and computed lateral pressure head profiles. Note: Absolute residuals are calculated as the absolute difference between computed measured pressures heads expressed as percentage of the measured pressure heads.

| Data-set | Lateral inlet discharge |                 | Absolute residuals (%) |
|----------|-------------------------|-----------------|------------------------|
|          | Measured (L/s)          | Simulated (L/s) |                        |
| 1        | 50.7                    | 55.2            | 8.8                    |
| 2        | 51.4                    | 55.2            | 7.5                    |
| 3        | 53.5                    | 55.2            | 3.3                    |

**Table 4:** Measured and computed lateral inlet discharges and residuals. Note: Absolute residuals are calculated as the absolute difference between computed and measured lateral inlet discharges expressed as a percentage of the measured discharges.

between the simulated and measured pressure head profiles. The maximum absolute residuals may not be considered low. However, a comparison of the average and maximum absolute residuals, obtained for each data-set, suggests that the maximum absolute residuals may not be good indicators of the overall error levels in the computed pressure head profiles. In fact, it can be shown that if the pair of measured pressure heads corresponding to the maximum absolute residuals are excluded from the respective pressure head profiles, the maximum residuals would be reduced from 14.3 to 8.8% for data-set 2 and from 16 to 8.5% for data-set 3.

**Comparison of measured and simulated lateral inlet discharges:** The measured and model predicted lateral inlet discharges for data-sets 2 and 3 are summarized in Table 4. The measured lateral inlet discharges are 51.4 L/s for data-set 2 and 53.5 L/s for data-set 3. By comparison, for both data-sets 2 and 3 the simulated inlet discharge is 55.2 L/s. The corresponding absolute residuals between the measured and simulated inlet discharges are 7.5 and 3.3% for data-sets 2 and 3, respectively, which suggests a satisfactory agreement between measurements and model predictions.

**Lateral-wide operating scenarios of the prvs:** To gain some insight on the possible sources of the differences between the measured and computed lateral inlet discharges, the simulated lateral-wide operating scenarios of the *prvs* corresponding to all the three data-sets used in model evaluation are examined here. As can be noted from Table 4, the measured lateral inlet discharges for data-sets 1, 2, and 3 vary between 50.7 and 53.5 L/s. By contrast, the simulated lateral inlet discharge for all the data-sets is 55.2 L/s.

The profiles of the minimum required inlet pressure heads for the *prvs* to operate reliably in the active mode,  $h_{min}$ , the simulated *prv*-inlet pressure heads,  $h_u$ , and sprinkler discharges,  $Q_s$ , for data-sets 1, 2, and 3 are depicted in Figure 3. Note that  $h_{min}$  is defined in manuscript I as the sum of the *prv*-set pressure,  $h_{prv}$ , and the minimum required margin between  $h_u$  and  $h_{prv}$  for the *prv* to operate reliably in the active mode,  $\delta h_{prv}$ . The values of  $h_{prv}$  and  $\delta h_{prv}$  for the *prvs* used in the lateral are given in Table 2 and the  $h_u$  and  $Q_s$  profiles are outputs of hydraulic simulations.

As can be noted from Figure 3, for all the data-sets the simulated  $h_u$  exceeds  $h_{min}$  over the entire lateral length. Furthermore, a close look at the simulated  $h_u$  profiles of data-sets 1 to 3 show that the maximum  $h_u$  is 26.8 m (data-set 3), which is well below the 90 m threshold given in Table 2 as the maximum allowable inlet pressure head for the *prv* to operate reliably in the active mode,  $h_{max}$ . This indicates that for each of the data-sets,  $h_{min} < h_u < h_{max}$  over the entire lateral length. The implication is that, for each data-set, all the *prvs* in the lateral were operating in the active mode and hence the *prv*-outlet pressure head was constant along the lateral and was equal to the *prv*-set pressure,  $h_{prv}$ , which was 4.2 m. The corresponding constant sprinkler discharge along the lateral was 0.158 L/s (Figure 3). This shows that the lateral inlet discharge of 55.2 L/s, computed for each of the data-sets, corresponds to a hydraulic scenario in which all the *prvs*, in the lateral, were operating in the active mode. On the other hand, the slightly lower measured lateral inlet discharges, compared to the discharge required for all the *prvs* in the lateral to be considered active, suggest that during the field evaluations some of the *prvs* in the lateral may have actually been operating in the passive mode. However, it ought to be noted that the differences between the measured and simulated lateral inlet discharges could at least partly be attributed to measurement errors, errors related to accuracy of pressure regulation, and possibly to some malfunctioning *prvs* and/or sprinklers.

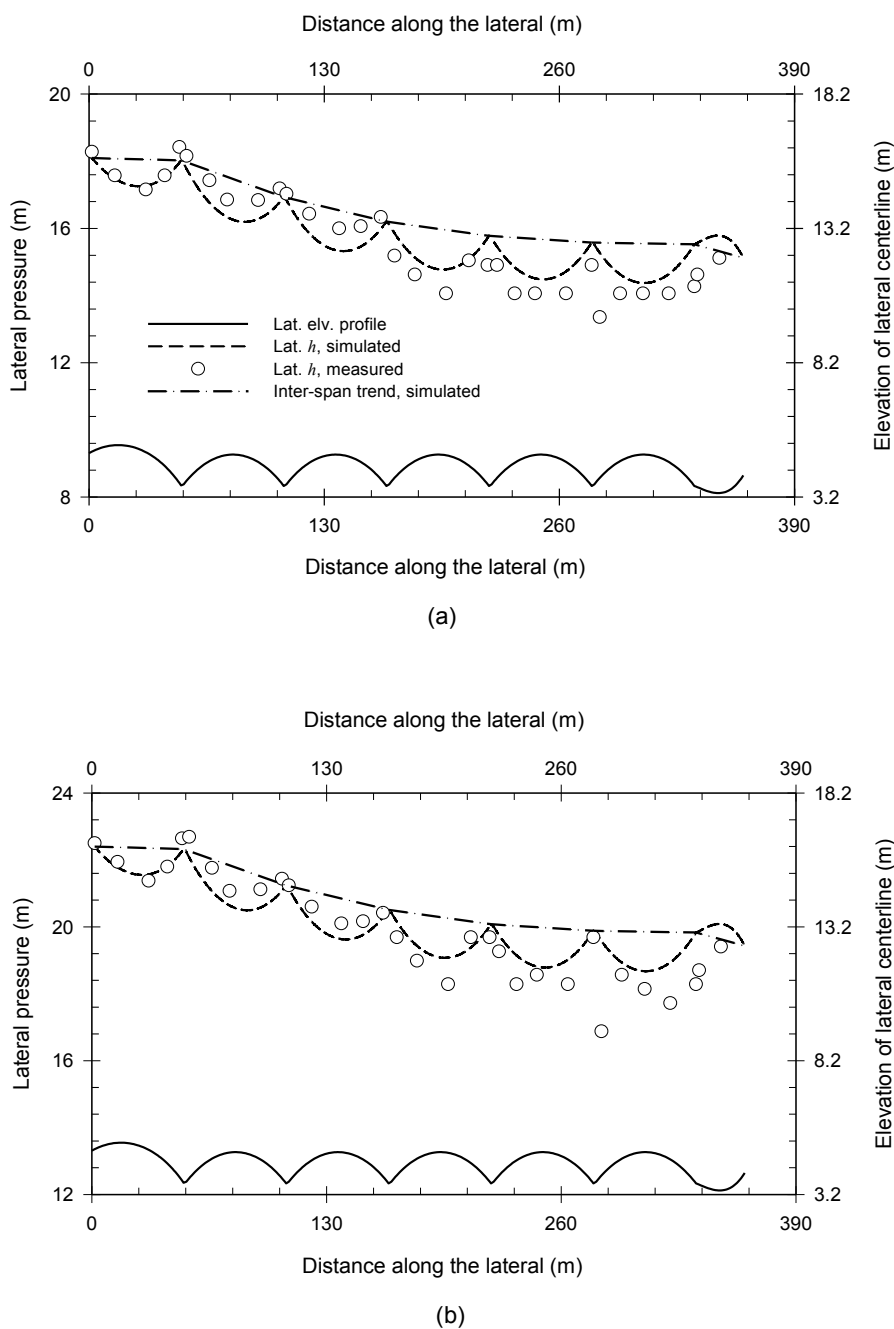


Figure 2: Comprison of measured and simulated lateral pressure head profiles: (a) Data-set 2 (inlet head of 23.4 m) and (b) Data-set 3 (inlet head of 27.7 m).

## Application Examples

The simulation examples presented here show potential applications of the hydraulic simulation model in analyzing *prv*-set pressure effects on lateral-wide *prv* operating scenarios and, possibly, in the selection of a suitable *prv*-set pressure for a lateral with a given set of hydraulic, geometric, and elevation profile attributes.

The simulation results summarized in Figure 3 suggest that, for each of the hydraulic scenarios considered, all the *prvs* in the lateral were operating in the active mode and hence the corresponding sprinkler discharge profiles were invariant with distance from the

lateral inlet. However, it is important to recognize here that this observation is specific to the parameter sets of the lateral used in the simulation. In general, it is conceivable that the operating modes of *prvs* in an irrigation lateral can vary along the lateral depending on the lateral parameter set. Based on the definition of the operating modes of *prvs* presented in the companion paper, it can be inferred that the lateral-wide operating scenarios of *prvs* fall into one of the following three categories:

(i) *Active*: a scenario in which  $h_{min} \leq h_u \leq h_{max}$  over the entire length of a lateral and hence all the *prvs* in a lateral are operating in the active mode,

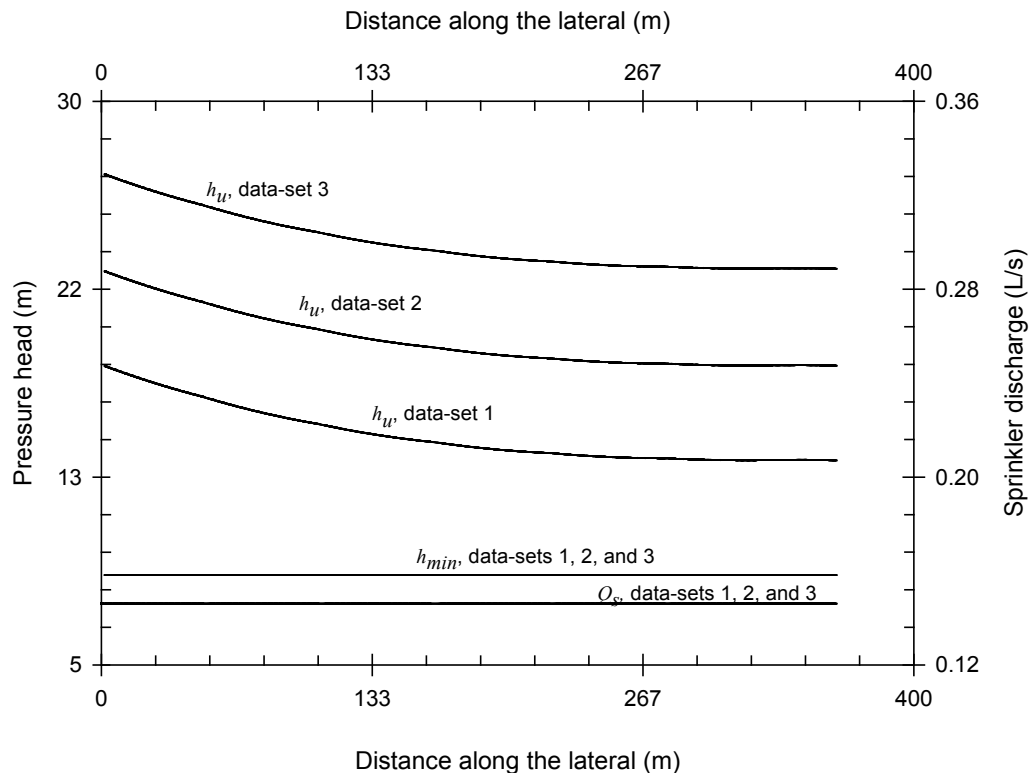


**Figure 3:** Comparison of  $h_{min}$ ,  $h_u$ , and  $Q_s$  profiles of the data-sets used in model evaluation (Notations:  $h_{min}$  is the minimum required inlet pressure head for the *prv* to operate reliably in the active mode,  $h_u$  is the simulated *prv*-inlet pressure head, and  $Q_s$  is the computed sprinkler discharge).

(ii) *Passive*: a scenario whereby  $h_u < h_{min}$  over the entire lateral length and as such all the *prvs* in a lateral are operating in the passive mode, and

(iii) *Mixed*: a scenario in which some of the *prvs* on a lateral are operating in the active mode (where  $h_{min} \leq h_u \leq h_{max}$ ) and some are operating in the passive mode (where  $h_u < h_{min}$ ). Note that additional categories are possible, if the fully-throttled operating mode of *prvs* (where  $h_{max} < h_u$ ) is considered. However, given that the fully-throttled mode is not permissible in a well-managed and properly functioning linear-move system, it is not considered here.

To further explore the variations in the lateral-wide operating scenarios of *prvs*, identified above, six example simulations were conducted based on data-set 1 (Tables 1 and 2). Noting that *prv*-set pressure,  $h_{prv}$ , is a key parameter in modeling the effects of *prvs* on lateral hydraulics (may note discussion in manuscripts I and II). Variations in lateral-wide operating scenarios of *prvs* were evaluated as a function of  $h_{prv}$ . Accordingly, each example simulation was conducted with a different  $h_{prv}$  while keeping all other lateral parameters constant at the level set in Tables 1 and 2. The *prv*-set pressures,  $h_{prv}$ , considered in the current analysis were 7.5, 7.8, 8.8, 11, 13, and 14.5 m. The lower and upper limits of the  $h_{prv}$  interval were set such that the resultant hydraulic scenarios cover the full range of variation of the lateral-wide operating modes of *prvs* given above.

### Results of simulation examples

First, consider the simulation example corresponding to the lower limit of the  $h_{prv}$  range, which is 7.5 m. As can be noted from Table 2, the minimum required margin, between  $h_u$  and  $h_{prv}$ , for proper functioning of the *prv* in the active mode,  $\delta h_{prv}$ , is 3.5 m. Thus, the corresponding

$h_{min}$  is 11 m. Figure 4a depicts the  $h_{min}$  profile superimposed on the simulated profiles of the *prv*-inlet pressure,  $h_u$ , sprinkler discharge,  $Q_s$ , and the *prv*-outlet pressure, which is the same as the sprinkler pressure,  $h_s$ . A closer look at the simulated data shows that the  $h_u$  profile, in Figure 4a, lies above the corresponding  $h_{min}$  profile (i.e.,  $h_{min} < h_u$ ) over the entire length of the lateral. Furthermore, the maximum of the simulated  $h_u$  profile (which occurs at the lateral inlet) is 18.1 m, which is well below the  $h_{max}$  value of 90 m, Table 2. The implication is that for this example the *prv*-inlet pressure,  $h_u$ , varies in the range  $h_{min} \leq h_u < h_{max}$ , hence the simulation example represents a scenario in which each of the *prvs* in the lateral are operating in the active mode. Accordingly, the outlet pressure of each of the *prvs* is a constant equal to the set pressure (which is 7.5 m) and the corresponding constant sprinkler discharge along the lateral is 0.211 L/s.

Now consider the  $h_{min}$ ,  $h_u$ ,  $Q_s$ , and  $h_s$  profiles obtained for an  $h_{prv}$  of 7.8 m (Figure 4b). Noting that  $\delta h_{prv}$  is kept constant at 3.5 m, it can be observed that as  $h_{prv}$  is increased from 7.5 to 7.8 m, the corresponding  $h_{min}$  increased from 11 to 11.3 m. Figure 4b shows that  $h_{min}$  for the current example falls within the range of variation of the corresponding *prv*-inlet pressure,  $h_u$ , and hence the  $h_{min}$  and  $h_u$  profiles intersected somewhere along the lateral between the inlet- and distal-ends.

The intersection point of  $h_{min}$  and  $h_u$ , which is marked by a vertical dash-dot-dot line in Figure 4b, is located at a distance of about 231.6 m from the inlet and it divides the lateral into two segments with contrasting *prv* operating modes. Accordingly, over the upper 231.6 m long reach of the lateral, which contains 221 of the *prv*-sprinkler assemblies, the actual *prv*-inlet pressure is within the interval  $h_{min} < h_u < h_{max}$ . The implication is that the first 221 *prvs*, from the lateral inlet, are operating in the active mode and hence the sprinkler pressure head

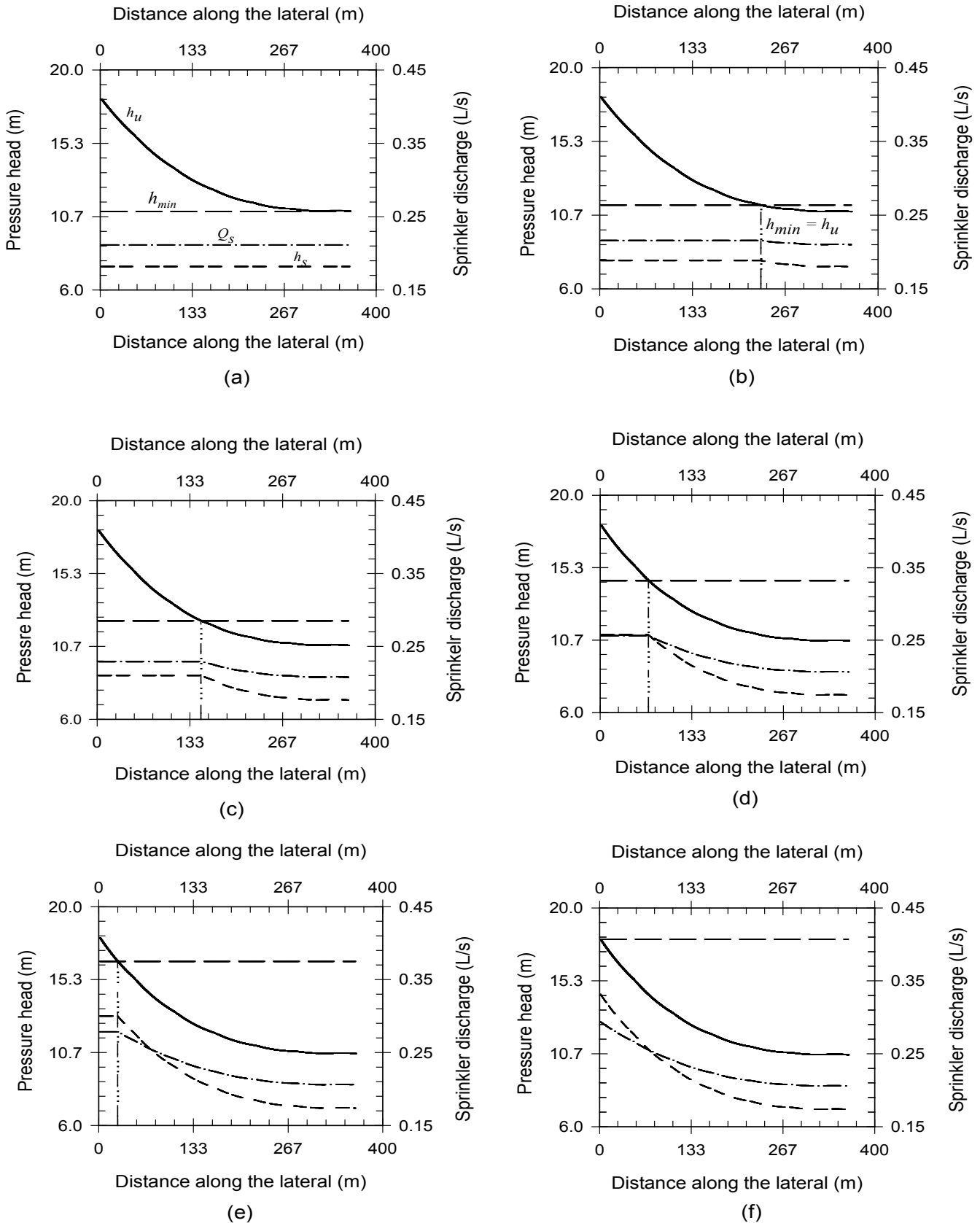


Figure 4: Effect of variations in  $h_{prv}$  on lateral-wide prv operating scenarios, for prv-set pressures of: (a) 7.5 m, (b) 7.8 m, (c) 8.8 m, (d) 11 m, (e) 13 m and (f) 14.5 m (Notations:  $h_{min}$  is the minimum inlet pressure required for an active prv;  $h_u$  is simulated prv-inlet pressure;  $h_s$  is prv-outlet pressure; and  $Q_s$  is sprinkler discharge).

over this lateral segment is a constant equal to the *prv* set pressure, which is 7.8 m (Figure 4b). The corresponding sprinkler discharge is also constant and is equal to 0.216 L/s. By comparison, over the lower 130.1 m long reach of the lateral, where the remaining 128 *prv*-sprinkler assemblies are,  $h_u$  is less than  $h_{min}$ . Thus, the *prvs* in this lateral segment operate in the passive mode. The *prvs* are fully open and no longer functioning as pressure regulators. As a result, the attached sprinklers interact directly with the system hydraulics upstream and hence the corresponding sprinkler pressure and discharge profiles are variable (i.e., they are decreasing functions of distance from the lateral inlet). Note that this example represents a mixed lateral-wide *prv* operating scenario. The total lateral inlet discharge is 74.7 L/s.

The  $h_{min}$ ,  $h_u$ ,  $Q_s$ , and  $h_s$  profiles corresponding to  $h_{prv}$  values of 8.8, 11, and 13 m are shown in Figure 4c, 4d, and 4e, respectively. For these examples, as  $h_{prv}$  is varied from 8.8 to 13 m the corresponding  $h_{min}$  increased from 12.3 to 16.5 m. Furthermore, it can be observed that for each of these simulation examples,  $h_{min}$  equals  $h_u$  somewhere along the lateral in between the inlet- and distal-ends (Figure 4c-4e). As a result, in each case the lateral consists of two segments characterized by different *prv*-operating modes. An upstream segment, with an active set of *prvs*, spanning the distance between the lateral inlet and the point of intersection of the  $h_{min}$  and  $h_u$  profiles and a downstream section, covering the distance between the intersection point of the  $h_{min}$  and  $h_u$  profiles and the distal-end of the lateral, where *prvs* are operating in the passive mode. Thus, the lateral-wide *prv* operating scenarios of each of these examples is mixed and is the same as that of the example presented in Figure 4b. Furthermore, it can be observed that as  $h_{prv}$  is increased from 8.8 to 13 m, the number of *prvs* that are operating in the active mode steadily decreased from 143 to 25 and the lateral inlet discharge increased from 76.7 to 80.0 L/s.

Finally, as the *prv*-set pressure is increased to 14.5 m, which is the upper limit of the  $h_{prv}$  range considered here, the corresponding  $h_{min}$

increased to 18 m. Furthermore, a closer look at the simulated data shows that the  $h_u$  profile, in Figure 4f, lies below the constant  $h_{min}$  profile (i.e.,  $h_{min} < h_u$ ) over the entire lateral length. The implication is that all the *prvs* in the lateral are fully open and hence operate in the passive mode. Thus, the corresponding lateral-wide operating modes of *prvs* are passive. As indicated in manuscript II, the hydraulics of such a system is the same that of a lateral without a *prv*. Accordingly, the *prv*-outlet pressure is variable along the lateral and is different from  $h_{prv}$  (Figure 4f). The corresponding  $Q_s$  profile varies between a minimum of 0.206 L/s at the distal-end and a maximum of 0.294 L/s at the inlet-end of the lateral. The lateral inlet discharge is 80.2 L/s.

### Discussion of simulation examples

#### General observations on the results of the simulation examples:

A closer examination of the simulated data, for Figure 4a, reveals that at the distal-end of the lateral  $h_u$  exceeds  $h_{min}$  only by 0.01 m (which is less than 0.1% of  $h_{min}$ ), thus the corresponding  $h_{prv}$ , which is 7.5 m, can be considered as an approximate threshold pressure at or below which the lateral-wide operating scenarios stay active. Similarly, the simulated data corresponding to Figure 4f shows that at the inlet end of the lateral  $h_{min}$  exceeds  $h_u$  by only about 0.03 m (which is less than 0.2% of  $h_{min}$ ), thus the corresponding  $h_{prv}$ , which is 14.5 m, can be considered as an approximate threshold set pressure at or above which lateral-wide *prv* operating scenarios remain passive. In between the threshold set pressures of 7.5 and 14.5 m, on the other hand, the simulation results show that the lateral-wide operating scenarios of the *prvs* will be comprised of some mix of both active and passive states. The observations summarized here show that the simulation model, presented in the companion paper, can potentially be used in the selection of an acceptable *prv*-set pressure for a lateral with a given combination of hydraulic, geometric, and elevation profile attributes. It is, however, important to note here that the selection of *prv*-set pressure needs to take into account the hydraulic characteristics of the

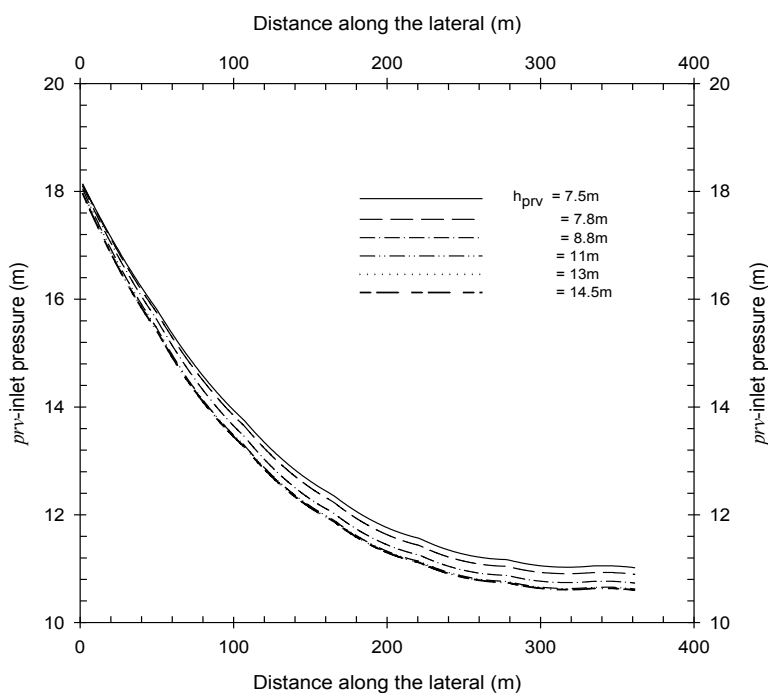


Figure 5: Comparison of the *prv*-inlet pressure,  $h_u$ , profiles for the example simulations presented in Figure 4.

attached sprinkler. Thus, there needs to be sufficient overlap between the range of variation of  $h_{prv}$  considered in the evaluation and the optimal operating pressure head range of the sprinkler.

The simulation results presented earlier also show that each of the examples, that involve a mixed lateral-wide *prv* operating scenario (Figure 4b-4e), consist of only two lateral segments with contrasting *prv* operating modes: an upstream segment with an active set of *prvs* followed by a downstream section comprised of a passive set of *prvs*. However, it ought to be pointed out that the observation regarding the number of active and passive segments, in a lateral with a mixed lateral-wide operating scenario, and the relative positions of the active and passive segments, along the lateral, are related to the specific lateral parameter set considered here and hence do not imply a general inference. In fact, it can be readily reasoned that depending on the lateral parameter set, particularly the field slope, the number of active segments on a lateral can exceed one. Note that the same can be said of the number of passive segments in a lateral. Furthermore, the relative positions of the active and passive segments, along a lateral, could be different from what is observed in the examples presented here.

**Description of the mechanism by which variations in  $h_{prv}$  affect lateral-wide *prv* operating scenarios:** Results of the simulation examples presented earlier show that increasing  $h_{prv}$  over a preset interval, while keeping all other factors constant, leads to a steady decrease in the fraction of active *prvs* in the lateral (Figure 4a-4f). Note that the fraction of active *prvs* in a lateral is defined here as the number of *prvs* in a lateral that are active, expressed as a percentage of the total number of *prvs* in the lateral. Accordingly, it can be observed that the fraction of active *prvs* in the lateral decreased from 100 (Figure 4a) to 0% (Figure 4f) as  $h_{prv}$  is increased from 7.5 to 14.5 m, while keeping all other factors constant. The simulation results also show that for a given  $h_{prv}$ , it is the location of the intersection point of the  $h_u$  and  $h_{min}$  profiles along the lateral that determines the extent of the active and passive segments of the lateral and hence the fraction of active *prvs* in the lateral. This implies that the observed steady decrease in the fraction of active *prvs* in the lateral, as  $h_{prv}$  increases, is related to the effects of  $h_{prv}$  on the  $h_{min}$  and  $h_u$  profiles.

As can be noted from the definition of  $h_{min}$  given in the companion paper, increasing the *prv*-inlet pressure,  $h_{prv}$ , leads to an increase in  $h_{min}$  by exactly the same amount as the corresponding increment in  $h_{prv}$ . Accordingly, as  $h_{prv}$  is increased, over the interval  $7.5 \text{ m} \leq h_{prv} \leq 14.5 \text{ m}$ , the  $h_{min}$  profile shows a steady upward shift (Figures 4a-4f). Furthermore, a closer look at the simulated data reveals that as  $h_{prv}$  is increased over the preset interval, the simulated  $h_u$  profiles exhibit a small, nonetheless, steady downward shift, mainly due to increased discharge and hence friction head loss along the lateral. To show this trend, among the simulated  $h_u$  profiles, the  $h_u$  profiles corresponding to each  $h_{prv}$  are depicted in a separate chart in Figure 5. It can, thus, be reasoned that as  $h_{prv}$  is increased over its preset interval, the location of the point at which  $h_{min} = h_u$  shifts steadily upstream along the lateral and hence the fraction of the active *prvs* on the lateral decreases, because of the combined effects of the consequent upward shift in  $h_{min}$  and the downward shift in  $h_u$  (Figures 4a-4f and 5). In other words, the length of the lateral segment with active *prvs* shrinks and the fraction of the active *prvs* in the lateral decreases as  $h_{prv}$  increases over its preset interval, because of the combined effects of the resultant upward shift in  $h_{min}$  and downward shift in  $h_u$ .

**Sensitivity of the fraction of active *prvs* in a lateral to variation  $h_{prv}$ :** A close look at the simulation results summarized in Figure 4a-4f

shows that the rate of change of the fraction of active *prvs*, in the lateral, with respect to changes in  $h_{prv}$  varies over the  $h_{prv}$  interval considered here. Overall, it can be observed that the fraction of active *prvs*, in the lateral, decreases at a decreasing rate as  $h_{prv}$  is increased over its preset range. A closer look at the simulated data for instance shows that increasing the *prv*-set pressure only by 1.3 m, from a lower limit of 7.5 to 8.8 m, leads to a 59% decrease in the fraction of active *prvs* (from 100% to 41%), Figure 4a-4c. This represents an average rate of decrease of 45.4%, in the fraction of active *prvs*, per meter change in the  $h_{prv}$ . By comparison, at the other end of the  $h_{prv}$  range, increasing  $h_{prv}$  by 5.7 m from 8.8 to 14.5 m leads only to a 41% decrease in the fraction of active *prvs* on the lateral, which represents an average rate of change of 7.2% in the fraction of active *prvs* per meter change in  $h_{prv}$ . The implication is that the fraction of active *prvs* shows a high degree of sensitivity to changes in  $h_{prv}$  in the lower segment of the  $h_{prv}$  range (i.e.,  $7.5 \text{ m} \leq h_{prv} \leq 8.8 \text{ m}$ ) and is less sensitive to variations in  $h_{prv}$  over the upper section of the  $h_{prv}$  range (i.e.,  $8.8 \text{ m} < h_{prv} \leq 14.5 \text{ m}$ ).

It can be shown that the variation in the sensitivity of the fraction of active *prvs*, in the lateral, to changes in  $h_{prv}$  is mainly a function of the nonlinear behavior of the  $h_u$  profile. The slope of the  $h_u$  profile is highest at the lateral inlet and then generally decreases with distance from inlet. This variability pattern in the slope of the  $h_u$  profile along the lateral is the key factor that modulates the sensitivity of the fraction of active *prvs* to changes in  $h_{prv}$ . Note that the lower section of the  $h_{prv}$  range ( $7.5 \text{ m} \leq h_{prv} \leq 8.8 \text{ m}$ ), where the fraction of active *prvs* show a high degree of sensitivity to variation in  $h_{prv}$ , corresponds to the simulation examples for which the equivalence point of  $h_{min}$  and  $h_u$  falls within the lower 212.6 m long reach of the lateral (Figure 4a-4c). In this segment of the lateral, which accounts for approximately the lower 59% of the lateral length, the slope of the  $h_u$  profile is relatively low (Figure 4a-4f). As a result, relatively small changes in  $h_{prv}$ , and hence  $h_{min}$ , leads to appreciable changes in the location of the point along the lateral at which  $h_{min} = h_u$  and to a significant change in the fraction of active *prvs* in the lateral. This evidently explains the observed relatively high sensitivity of the active fraction of *prvs* in the lateral to variations in  $h_{prv}$  over the interval  $7.5 \text{ m} \leq h_{prv} \leq 8.8 \text{ m}$ .

By contrast, the upper segment of the  $h_{prv}$  range considered here (i.e.,  $8.8 \text{ m} < h_{prv} \leq 14.5 \text{ m}$ ), where the fraction of active *prvs* show a low degree of sensitivity to variation in  $h_{prv}$ , corresponds to the simulation examples for which the equivalence point of  $h_{min}$  and  $h_u$  falls within the upper 149.1 m long reach of the lateral (Figure 4c-4f). In this lateral segment, which accounts for about the upper 41% of the lateral, the slope of the  $h_u$  profile is comparatively high. Consequently, relatively large changes in  $h_{prv}$ , and hence  $h_{min}$ , leads only to smaller changes in the location of the point along the lateral at which  $h_{min} = h_u$  and hence in the fraction of active *prvs* in the lateral. In other words, if  $h_{prv}$  is set such that the resultant  $h_{min}$  equals the simulated  $h_u$  within the upper 41% of the lateral length, then the relatively high slope of the  $h_u$  profile over this segment of the lateral significantly dampens the sensitivity of the fraction of active *prvs* in the lateral to variation in  $h_{prv}$ . Note that this explains the relatively low sensitivity of the active fraction of *prvs* to changes in  $h_{prv}$  over the interval  $8.8 \text{ m} < h_{prv} \leq 14.5 \text{ m}$ .

Note that the preceding discussion on the sensitivity of the active fraction of *prvs* to variations in  $h_{prv}$  did not explicitly consider the effect of  $h_{prv}$  on the  $h_u$  profile. In other words, the  $h_u$  profile is treated as though it is insensitive to changes in  $h_{prv}$ . As can be noted from the results presented earlier, the  $h_{min}$  profile exhibited a significantly higher degree of sensitivity to changes in  $h_{prv}$  than the  $h_u$  profile. The implication is that the sensitivity of the active fraction of *prvs* to variations in  $h_{prv}$

is largely dictated by the effect of  $h_{prv}$  on  $h_{min}$ . Thus, in the interest of simplicity, the discussion here is focused on the effects of  $h_{prv}$  on  $h_{min}$  and ignored the relatively negligible effects of  $h_{prv}$  on the  $h_u$  profile.

## Summary and Conclusions

This manuscript is the third part of a three-part article which presents a hydraulic simulation model for linear-move sprinkler irrigation systems equipped with pressure reducing valves (*prvs*). In part-one of the paper system configuration and components, model assumptions, and specification of the lateral hydraulic simulation problem is discussed. Formulation and numerical solution of the lateral hydraulic simulation problem are described in part-two of the paper. Evaluations of the model and example simulations showing its potential applications in the analysis of linear-move sprinkler irrigation system hydraulics are presented here.

Model evaluation was conducted through comparisons of model outputs with field-measured hydraulic data. The data was obtained through field tests performed on a linear-move sprinkler irrigation system consisting of a series of arched spans, each with multiple outlet ports placed at variable spacing. The linear-move unit obtained its water supply from a concrete-lined canal and was operated under near steady flow conditions. Spray nozzles were used to apply water along the lateral. Each nozzle was coupled to a *prv* at its inlet end so as to maintain a set pressure upstream of the nozzle. Drop-tubes were used to convey water from the overhead outlet ports down to each *prv*-sprinkler assembly. Three data-sets, each consisting of lateral pressure head profile and lateral inlet discharge, were obtained through the field evaluations. One of the data-sets was used in parameter estimation and the remaining two were used in model verification, i.e., comparison of measured and simulated lateral pressure head profiles and inlet discharges. Considering the pair of data-sets used in model verification, the average percent absolute residuals between the simulated and measured pressure head profiles were 3 and 3.7%. Furthermore, the absolute residuals between the measured and computed lateral inlet discharges were 3.3 and 7.5%. Overall, the relatively low average absolute residuals, obtained for both the lateral pressure head profiles and inlet discharges, suggest that model performance is satisfactory.

Furthermore, application examples aimed at evaluating the effects of *prv*-set pressure on lateral-wide *prv* operating scenarios are presented. The results showed that increasing the *prv*-set pressure steadily starting from a sufficiently small value, while keeping all other factors constant, led to a decrease in the number of *prvs* in the lateral that were operating in the active mode. However, the rate with which the number of active *prvs* in a lateral decreased, in response to changes in the *prv*-set pressure, varied over the *prv*-set pressure range. It was most sensitive in the lower reaches of the *prv*-set pressure interval and was least sensitive in the upper section of the interval. Results of

the simulation examples also showed that the model can be used in the selection of a suitable *prv*-set pressure for a lateral with a given combination of hydraulic, geometric, and elevation attributes.

## References

1. Gregg T (2004) Water Conservation Best Management Practice Guide, Report 362, Texas Water Development Board, Austin, Texas.
2. Keller J, Corey F, Walker WR, Vavra ME (1980) Evaluation of Irrigation Systems. In Irrigation: Challenges of the 80's. Proceedings of the Second National Irrigation Symposium, 95-105, St. Joseph, MI, ASAE.
3. Christiansen JE (1942) Irrigation by Sprinkling. California Agricultural Experiment Station Bulletin, 670, University of California, Davis, CA.
4. Keller J, Bliesner R (1990) Sprinkle and trickle irrigation. Van Nostrand Reinhold, New York, NY.
5. Martin DL, Heermann DF, Madison M (2007) Design and Operation of Farm Irrigation Systems. In: Hoffmans GJ, Evans RG, Jensen ME, Martin DL, Elliott RL, (2<sup>nd</sup> eds.) Hydraulics of Sprinkler and Micro-Irrigation Systems American Society of Agricultural and Biological Engineers Chapter 15, pp. 532-555.
6. Kincaid DC, Heermann DF (1970) Pressure Distribution on a Center-Pivot Sprinkler Irrigation System. Trans ASAE, 13(5):556-558.
7. Chu ST, Moe DL (1972) Hydraulics of a Center Pivot System. Amer Soc Agr Eng Trans ASAE, 15(5):894-896.
8. Scaloppi EJ, Allen RG (1993) Hydraulics of Center-Pivot Laterals. J Irrig Drain Eng, ASCE 119(3): 554-567.
9. Fraisse CW, Heermann DF, Duke HR (1995) Simulation of Variable Water Application with Linear-Move Irrigation System. Transactions of the ASAE, 38(5):1371-1376.
10. Anwar AA (1999) Friction Correction Factors for Center-Pivots. J Irrig Drain Eng ASCE, 125(5): 280-286.
11. Valiantzas JD, Dercas N (2005) Hydraulic Analysis of Multidiameter Center-Pivot Sprinkler Laterals. J Irrig Drain Eng ASCE, 131(2): 137-142.
12. Heermann DF, Stahl KM (2006) CPED: Center Pivot Evaluation and Design. Center for Agricultural Resources Research, Water Management and Systems Research, USDA.
13. Tabuada MA (2014) Friction Head Loss in Center-Pivot Laterals with Single Diameter and Multidiameter. J Irrig Drain Eng, ASCE, 140(10): 04014033.
14. Hathoot HM, Abo-Ghobar HM, Al-Amud AI, Mohammad FS (1994) Analysis and Design of Sprinkler Irrigation Laterals. J Irrig Drain Eng ASCE, 120(3):534-549.
15. Zerihun D, Sanchez CA, Nolte K (2014) Field-scale Sprinkler Irrigation Hydraulic Model. I. Hydraulic Characterization. J Irrig Drain Eng (ASCE) 140(7): 04014019.
16. Zerihun D, Sanchez CA (2017) Irrigation Lateral Hydraulics with the Gradient Method. J Irrig Drain Eng ASCE, 143(8): 04017023.
17. Senninger (2015) Chart No. MK-923-13B. Senninger Irrigation Inc., Clermont, Florida.
18. Senninger (2017) Super Spray: Customizable Field Proven Technology, Agricultural Irrigation, Low Pressure - High Performance.
19. Senninger (2017) Pressure Regulator Guide, Agricultural, Residential & Commercial Irrigation, Low Pressure - High Performance.